Journal of Materials Processing Tech. 303 (2022) 117525

Contents lists available at ScienceDirect

Journal of Materials Processing Tech.

journal homepage: www.elsevier.com/locate/jmatprotec

Effect of high pressure die casting on the castability, defects and mechanical properties of aluminium alloys in extra-large thin-wall castings

Zhichao Niu, Guangyu Liu, Tian Li, Shouxun Ji *

Brunel Centre for Advanced Solidification Technology (BCAST), Brunel University London, Uxbridge, Middlesex UB8 3PH, United Kingdom

ARTICLE INFO

Keywords:
Aluminium alloys
Microstructres
Mechanical properties
High pressure die casting
Castability
Effective flow length (EFL)

ABSTRACT

The manufacturing of extra-large thin-wall castings using high pressure die casting is one of the most significant challenges for structural applications requiring excellent ductility. The present study aims to understand the effect of process parameters on the castability, defect formation and mechanical properties of aluminium alloys in extra-large thin-wall castings with a maximum flow length of 1230 mm in the 2.8 mm thick channel. Numerical simulation and experimental verification were carried out to tailor the process parameters in high pressure die casting. It is found that the process parameters can significantly affect the castability and mechanical properties of as-cast components. For a complete casting, the yield strength is slightly increased but the elongation is significantly decreased at the locations further away from runners. A new concept of effective flow length (EFL) is proposed and used to assess the castability in extra-large thin-wall high pressure die castings. Under the optimum casting condition, the EFL can reach 525 mm, at which the ratio of EFL to wall thickness is 187 and the yield strength and elongation are greater than 120 MPa and 10%, respectively. Although the extra-large thin-wall castings can be geometrically filled under several conditions, the heterogeneity of mechanical properties is the most significant concern, in which the variation of elongation is overwhelmingly important for the structural applications requiring excellent ductility under as-cast conditions. Therefore, the criteria of casting quality should consider both geometrical soundness and the homogeneity of mechanical properties in the casting body.

1. Introduction

Cast Al-Si-Mg alloys have been extensively utilized in transport manufacturing, particularly in the automobile industry because of their attractive physical and mechanical properties including high strength to weight ratio, superior wear and corrosion resistance, excellent castability, and low cost (Rowe, 2012). In the past twenty years, Al-Si-Mg die castings are increasingly developed for structural components with thin-wall and complex geometries due to high productivity, relatively low cost, excellent mechanical properties and acceptable castability (Niu et al., 2000; Ji et al., 2012). These structural die castings are often used after solutionisation and ageing treatment to achieve excellent mechanical properties with exceptional ductility. However, heat treatment always consumes energy, increases manufacturing costs and causes distortion in large and thin-wall components (Zhu et al., 2021). Recently, the extra-large thin-wall castings made by high ductile Al-Si-Mg alloys is highly desirable for the application under as-cast condition because of the advantages in dimensional accuracy and surface finishing, cost benefits and short manufacturing route without heat treatment.

The castability of high pressure die casting (HPDC) alloys was reported to be principally related to the die temperature, the in-gate velocity of melt, and casting pressure (Kong et al., 2008). It was found that the combination of die temperature, the mould filling capacity of molten metal, the geometrical complexity of parts and cooling rate during die casting significantly affect the integrity of cast components. Similar results was found from the simulation results carried out by Cleary et al. (2006) and Kong et al. (2008). In addition, the slow forwarding speed of melt in the shot sleeve was found to be able to minimize the gas entrainment in the HPDC process and increase the mechanical properties of castings (Barkhudarov and President, 2009, Dou et al.,2021). Different runners and ventings lead to different melt flow, heat transfer and solidification in die cavity (Gunasegaram et al., 2013). Meanwhile, Dong et al., (2019, 2020) found that the application of vacuum during HPDC can significantly improve the mechanical properties of aluminium alloys and MMCs. Therefore, the optimization of process parameters is

* Corresponding author.
E-mail address: shouxun.ji@brunel.ac.uk (S. Ji).

https://doi.org/10.1016/j.jmatprotec.2022.117525
Received 20 October 2021; Received in revised form 19 January 2022; Accepted 4 February 2022
Available online 8 February 2022

an effective and essential approach to control the mechanical properties of castings. However, current researches mainly focus on castability using the criterion of geometrical soundness. Little information is available for the heterogeneity of mechanical properties in extra-large thin-wall castings in terms of synergetic assessment of castability, defects and mechanical properties. Moreover, the comparable assessment between numerical simulation during design and real casting components for fluid flow, defect formation and the heterogeneity of mechanical properties of extra-large castings is still rare, although it is extremely important in the manufacturing of new EV structures.

This work aims to understand the castability, defect and heterogeneity of mechanical properties of die-cast Al-Si-Mg alloys in extra-large thin-wall castings. A systematic experimental study was carried out using a 16000 kN vacuum-assisted cold chamber die casting cell and a set of the purposely designed die to make castings with a dimension of 1230 × 220 × 2.8 mm. Numerous casting trials and comprehensive analyses on the complex casting process were performed to explore the effect of varied process parameters including melt temperature, die temperature, and cavity fill time (in-gate velocity), on the microstructure, mechanical properties and defects in castings. Based on the comprehensive assessment for the geometrical soundness, defects, microstructural feature and mechanical properties in different locations of castings, a new concept of effective flow length (EFL) was proposed for better describing the nature of castability in extra-large thin-wall high pressure die castings. The discussion focuses on the relationship between the process parameters, defect formation, microstructural evolution and mechanical properties of die castings.

2. Simulation and experimental

2.1. HPDC cell

Fig. 1 shows the fully automatic HPDC system for producing the extra-large thin-wall castings. The key equipment includes a Frech 16,000 kN vacuum-assisted cold chamber machine, a 800 kg electric heating furnace and an automatic dosing system, an ABB robotics, an automatic spraying system and 3 heating/cooling machines. These equipment are coherently integrated to form an automatic cell with the capability of acquisition of process parameters for whole manufacturing cycles of HPDC. In addition, two thermal cameras are equipped on the two half of the die for real-time temperature monitoring, as shown in Fig. 1(c).

2.2. Casting geometry, runner,and overflow design

A component designed for crash test of ductile materials was used to test the fluidity of target material in extra-large thin-wall castings. Flat plates and ribs with about 90-degree turning angle were designed to satisfy the requirement of real engineering products. With a casting of 635 × 220 × 2.8 mm, the real maximum flow length of die casting was

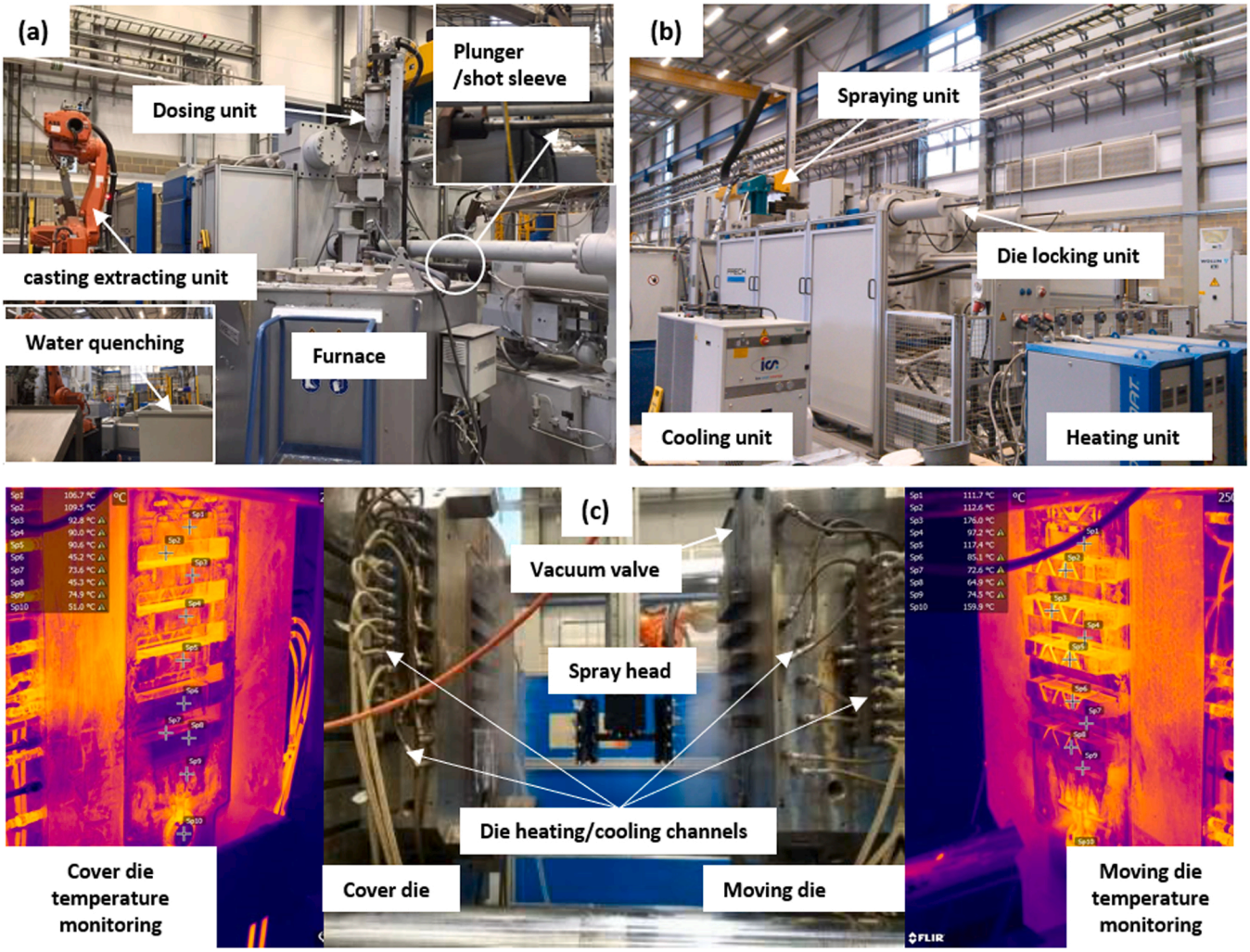

Fig. 1. Integrated fully automatic HPDC cell: (a) furnace, melt feeding and casting extraction; (b) heating, cooling and spraying units; (c) HPDC die and die temperature control systems.

1230 mm in the 2.8 mm thick channel. The runner system and overflows were designed, optimised and integrated with cooling and heating channels, vacuum system and spraying control. The inserts of the die were made by H13 tool steel with hardening to reach hardness HRC 52–55. Fig. 2 shows the structure and geometry of casting. The software to optimise runner and overflow from the results of melt filling and solidification was Magmasoft. The detailed simulation setup is shown in Table 1.

2.3. Materials preparation and casting process

The Al-Si-Mg alloy ingots used in the experimental trials were supplied by a commercial manufacturer. In each trial of casting, 800 Kg of alloy ingots were melted and held for approximately 2 h at 695 ± 5 °C

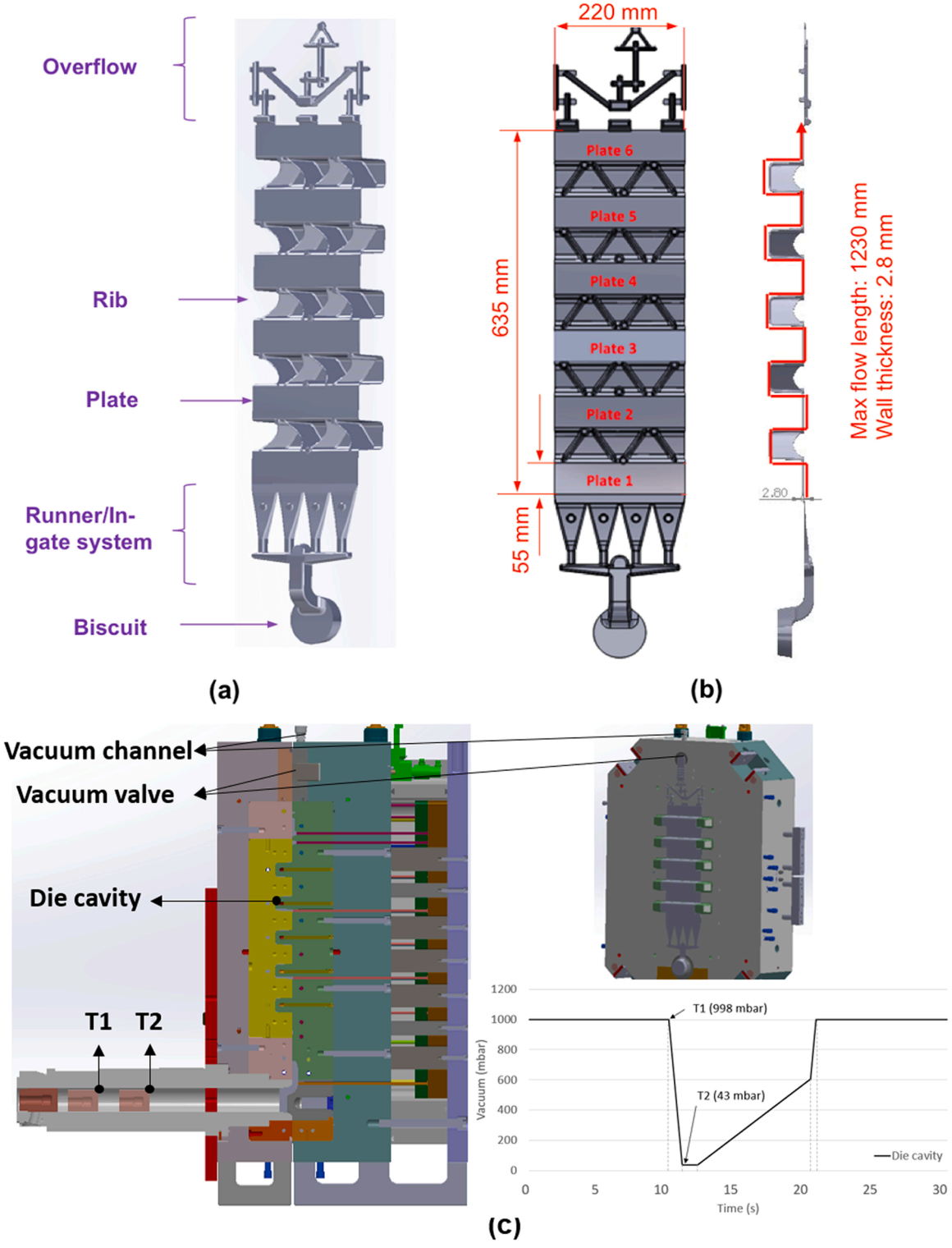

Fig. 2. 3D models and casting design for high pressure die castings, (a) models of different parts in the design, (b) geometry and schematic flow length of casting, (c) vacuum system and vacuum of full shot during the high pressure die casting process.

Table 1
Casting parameters used in the simulation of fluidity and solidification.

Parameter	Unit	Value
Alloy		AlSi7
Temperature oven	[°C]	719.70
Temperature shot sleeve	[°C]	619.00
Raw part weight	[g]	3522.00
Biscuit thickness	[mm]	25.00
Mean wall thickness	[mm]	2.80
Filling time	[ms]	79.00
Active length of shot sleeve	[mm]	792.00
Plunger diameter	[mm]	80.00
Shot sleeve filling ratio	[%]	33.22
Cavity pressure	[bar]	900.00
Vacuum section	[mm^2]	154.00
Plunger velocity phase 1	[m/s]	0.20
Plunger velocity phase 2	[m/s]	2.50
Die temperature	[°C]	200.00

for homogenisation, during which 0.2% of Al-10 wt%Sr master alloy was added to the melt. Then degassing was conducted with argon (Ar) to reach the required density index of < 0.5. During degassing, the melt was covered by a commercial granular flux (FOSECO Coveral GR 2532). Once density index was measured with satisfactory results, the melt was set for casting and the melt temperature was automatically controlled by the system. The chemical composition of the alloy after melt treatment was verified by inductively coupled plasma atomic emission spectroscopy (ICP-AES) using a standard mushroom sample (ø60 ×10 mm). About 3 mm thick alloys were cut off from the bottom of the mushroom sample and grounded using 400 grid paper before ICP-AES testing. The results are consistent and within the required ranges, as shown in Table 2.

The optimisation of casting parameters included in-gate velocity, melt temperature and die temperature. The evacuation process in a full shot diagram during high pressure die casting was shown in Fig. 2(c). It was conducted by a BUSCH vacuum system with ø600 * 1723 mm vacuum tank size, 1000 $m^3 h^{-1}$ vacuum pumping speed and a 35 mm diameter vacuum valve. The vacuum level was measured at the end of over flow outside the die cavity, while the gauge was placed as close to the valve in order to measure the actual die cavity vacuum pressure. During casting, the vacuum system was triggered automatically when the plunger tip passed the melt inlet in the shot sleeve at time T1 and the vacuum level in the die cavity was at the standard atmosphere of around 1000 mbar; vacuum was stopped just before the plunger accelerated for high speed shot at time T2, at which, the vacuum level in the die cavity decreased sharply due to the evacuation and was maintained at a level less than 50 mbar. After T2, the high speed shot and filling of the die cavity happened followed by rapid solidification under vacuum condition. The cooling time was optimized at 10 s. Other casting parameters were fixed as usual as the range of these were considered as negligible for a specific machine. In this study, the shot speeds were differentiated at 2.8, 4.0, and 4.8 m s^{-1} for the 3rd forwarding speed of the plunger, which was equivalent to the cavity fill time of 68.6, 51.4, 41.1 ms and in-gate velocity of 30, 40, 50 m s^{-1}, respectively at an 80 mm plunger diameter and 484 mm^2 gating area. The pouring temperatures of the melt were set to 700, 720, and 740 °C. The die temperatures were controlled at 100, 150, and 200 °C by an online controller fitted in each channel and the die body. During experiments, only one parameter was varied while the others were maintained unchanged to systematically explore the effect on the castability, microstructure, and mechanical properties of castings.

2.4. Mechanical tests

The flat samples for mechanical tests were taken from the center of the casting body on each plate. The geometry and dimension of samples are shown in Fig. 3. The tensile tests were conducted at room temperature (20 °C) according to ASTM E8/E8M using an Instron 5500 universal Electromechanical Testing System equipped with Bluehill software and a 50 KN load cell. The yield strength (YS), ultimate tensile stress (UTS), and elongation reported with standard deviations were obtained by the average value of 8 continuous castings under each condition to reduce the measurement uncertainty.

2.5. 2.5 Microstructure characterization

The microstructural examination was conducted on the cross-section of casting samples. The examining surface was ground using SiC abrasive papers and then polished using silica suspension (OPS, 0.05 μm water-based SiO_2 suspension). Information on the dendritic structure and porosities was analysed using a Zeiss Scope A1 optical microscope. Quantitative analysis of the microstructure was performed using AxioVision Rel. 4.8 software. Microstructural features for Si eutectic phase and intermetallic phase were characterised using the Zeiss Supra 35 field-emission scanning electron microscope (FESEM), equipped with energy-dispersive X-ray spectroscopy (EDS). Macro-CT (Zeiss Xradia 410 Versa X-ray) was employed to identify large porosities (>0.2 mm).

3. Results and discussion

3.1. Simulation of mould filling and solidification

Fig. 4 shows the simulation results for melt filling and solidification at die temperature of 200 °C, melt temperature of 720 °C and in-gate speed at a level of 50 m s^{-1} (cavity fill time of 41.1 ms). Fig. 4a and b show the material trace and temperature distribution throughout the casting from runners to overflows at 90% fill, and Fig. 4c shows the distribution of liquid fraction across the casting during solidification (at the overall liquid fraction of 55%). In general, during filling, the melt flowed from the runner and entered the cavity. After the cavity was fulfilled, the melt started to fill the overflows. As indicated in Fig. 4a, by highlighting the respective melt fractions from each in-gate in different colours, the “material trace” can show which portion of the melt in the casting passed through each in-gate on its way into the cavity, i.e., how the melt was distributed into the part, thus, making visible the distribution of the melt in the simulation. It was observed that throughout the filling of the die cavity, the melt displayed a uniform flow without obvious turbulent flow and air entrapment. Besides, it is worth mentioning that the rib structure had no significant impact to cause turbulent filling.

It is observed from Fig. 4b that the melt temperature was maintained at the runners and in-gate portions. The reduction of filling temperature was progressively away from the entrance. This indicates that no solidification occurred in the runners. During solidification, the melt near the overflows likely solidified first compared to the melt near runners due to the lower temperature, although it is prefered that the solidification in the die cavity occurred simultaneously. Fig. 4c shows that the melt fraction was decreased from plate 1 to plate 6. The difference in solidification could affect the mechanical properties of these plates. In addition, the areas near ribs solidified at the final stage, therefore, porosities might be formed in local areas. By comparing the simulation results under varied casting parameters, it was also found that a higher

Table 2
Chemical composition of the experimental Al-Si-Mg alloys measured by ICP-AES.

Element	Si	Fe	Mn	Mg	Ti	Ca	Sr	Cu	Al
Content (wt%)	6.70	0.07	0.51	0.20	0.07	< 0.001	0.012	0.01	Bal

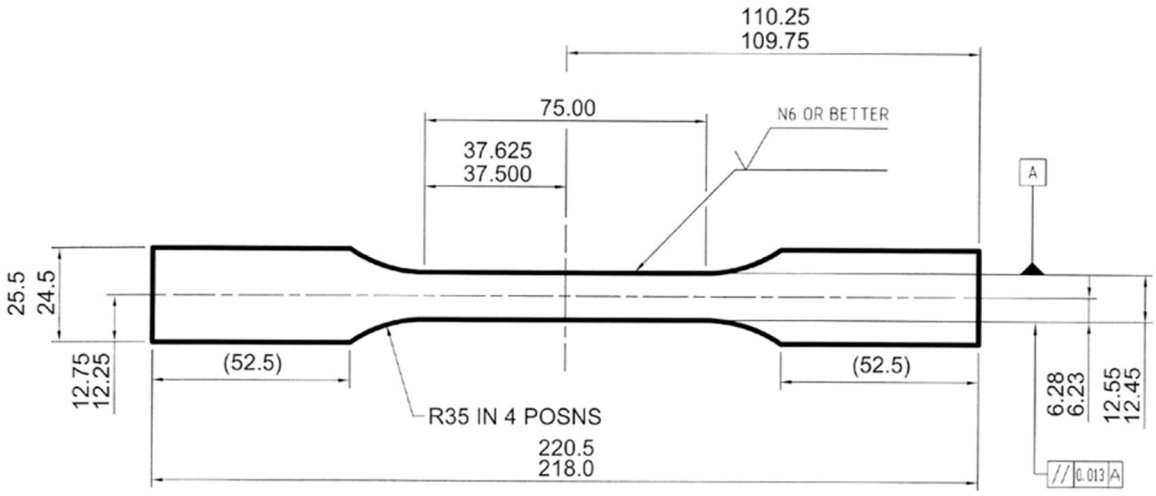

Fig. 3. The geometry and dimension of samples for tensile property testing.

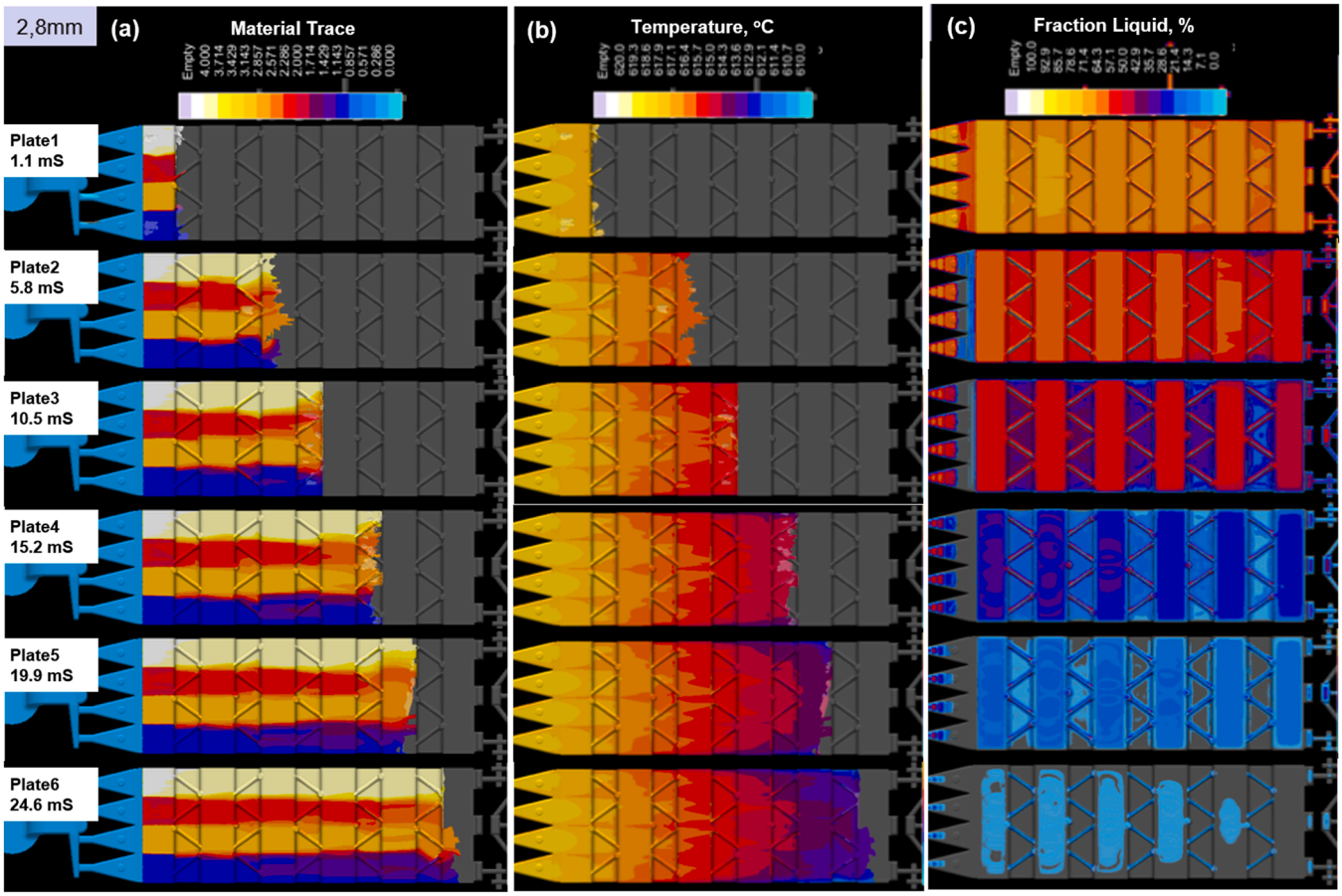

Fig. 4. Simulation results showing (a) the material trace, (b) the temperature at gradually filling of the die cavity, and (c) the liquid fraction distribution from biscuit to overflow with different overall liquid fractions during the solidification process, from plate 1 to plate 6, respectively.

melt temperature, higher die temperature and relative high in-gate velocity could increase the filling rate of the die cavity and reduce the porosity defects at a larger flow length. It needs to emphasise that the casting filling seems not a big issue when process parameters are carefully selected and controlled.

3.2. *Castability of Al-Si-Mg alloys in extra-large thin-wall castings*

Manufacture of extra-large thin-wall castings with complex structures using HPDC is extremely difficult due to the worsen fluidity originated from the decreased temperature of melt during filling. Considering the great length (1230 mm) of the casting part in the present study, castability becomes a critical factor to achieve the good quality of final products. During the manufacturing, purposely designed

experimental trials and analysis were conducted under varied parameters, as shown in Table 3.

These parameters were examed and controlled to address the challenges of consistent mechanical properties in extra-large thin-wall castings. The comprehensive analysis of the effect of process parameters on the castability is also summarised in Table 3. From the experimental results, it can be observed that castings can be made under several conditions, however, the casting of good quality with the largest flow length can only be obtained under a specific combination of process parameters. The process parameters optimised for the quality casting is highlighted in green in Table 3. The optimised shot weight was 3.9 kg, which could avoid the casting stacking inside the shot sleeve resulted from too much melt, or the difficulty for casting extraction by robotics due to small biscuit. The cooling time is optimised as 10 s by releasing temperature of casting, and monising the die soldering. The optimisation of spraying included the adjustment of spraying time and location, concentration of spray suspension, the type of lubricant and flow rate of spraying suspension. The other factors such as the intensification pressure of HPDC unit hydraulic system and die cavity pressure, which is effective pressure from plunger onto the melt, were optimised as well based on the process capability. It is found that three key parameters including shot speed, melt temperature and die temperature is significant for the fluidity and flow length in HPDC process to make extra-large thin-wall casting, which is evaluated and validated in the following section.

3.3. *Effects of melt temperature, die temperature and in-gate velocity on casting defects*

As a critical factor, castability usually refers to the capability of making sound casting, in particular the good finishing of geometry. Therefore, the influence of the casting parameters on the macro-scale defects such as cracks, misruns, surface flaws, and casting integrity was assessed. Fig. 5 shows the castings obtained at the cavity fill time of 41.1, 51.4, 68.6, 82.3 and 102.9 ms, which equivalent to the in-gate velocities of 50, 40, 30, 25, and 20 m s^{-1} at the same die temperature of 200 °C and melt temperature of 720 °C. At the cavity fill time of 41.1, 51.4 and 68.6 ms (in-gate velocity of 50, 40 and 30 m s^{-1}), complete castings containing the biscuit, runners and overflows can be obtained (Fig. 5a, b&c). However, when the in-gate velocities were decreased to 25 m s^{-1} and 20 m s^{-1}, the overflows were not fully filled (Fig. 5d) and even entirely unfilled (Fig. 5e). These indicate that, when the in-gate velocity was lower than 30 m s^{-1}(cavity fill time larger than 68.8 ms), it was unlikely to obtain a complete casting part. It was generally believed that the overflows could capture dirty melt and air entrapment. Without the fulfilling of overflow, the quality castings were not able to be obtained.

It was expected that the higher die and/or melt temperature would improve the fluidity and castability of the alloys and thus generating a complete casting at relatively lower in-gate velocities. Various casting trials were thus independently conducted at the die temperatures of 200 and 250 °C and the melt temperatures of 740 and 750 °C under the in-gate velocities less than 30 m s^{-1} (25 m s^{-1} and 20 m s^{-1}). The results showed a similar phenomenon that, when the in-gate velocity was lower than 30 m s^{-1}, no complete casting could be obtained despite the increased die and melt temperatures. This further proved that the in-gate velocity less than 30 m s^{-1} (cavity fill time larger than 68.8 ms) is not feasible to achieve complete extra-large thin-wall castings.

Fig. 6 presents the Macro-CT observations of the castings obtained at respective die and melt temperatures of 150 °C and 720 °C, and the cavity fill time of 51.4 and 41.1 ms/in-gate velocity of 40 and 50 m s^{-1} (Fig. 6a&b). No porosities larger than 0.1 mm (the highest resolution of the X-ray machine) was observed throughout the whole castings. Besides, as can be observed in the X-ray 3D image (Fig. 6c), minor defects indicated by the blue spots were present, which were primarily located in the vicinity of the inject pin areas (thickest locations in casting).

Table 3
Process parameters studied in HPDC of extra-large thin-wall parts.

Shot weight	[kg]	3.7	3.8	3.9	4.0	
Melt temperature	[°C]	740	720	700	690	
Die heating oil/cooling water	[°C]	Oil only	200	150	100	70
		Oil +Water	200+4 L/min	200+2 L/min	150+4 L/min	150+2 L/min	100+2 L/min
Cavity fill time	[ms]	102.9	82.3	68.6	51.4	41.1
In-gate velocity (shot speed)	[m/s]	20	25	30	40	50
Cooling time	[s]	6	8	10	12	
Die lubricant		Petrofer 4045	Chemtrend SL-2382	Trennex W 8000		
Die lubricant content	[%]	2	1.5	1	0.5	
Piston lubricant		High graphite content lube	Petrofer GF 35 (mineral oil)	30% GF 35 + 70% Norlube 1038		
Spray time + location		20s lubricant +air below throughout biscuit to overflow				
Die cavity pressure	[bar]	902				

Cannot continued casting (Die sticking issue etc.)
Casting quality not good (Visually defects or flow length less than 525mm)
Optimised casting parameters (Good quality for 525mm flow length)

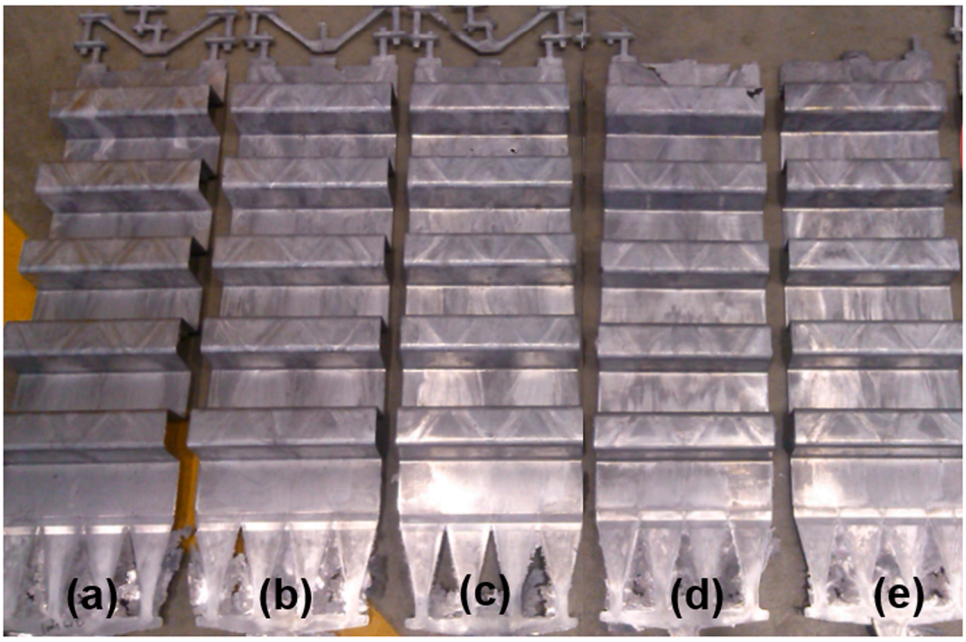

Fig. 5. Casting photos obtained at the die temperature of 200 °C and melt temperature of 720 °C, under different cavity fill time/in-gate velocities of (a) 41.1 ms/50 m s^{-1}, (b) 51.4 ms/40 m s^{-1}, (c) 68.6 ms/30 m s^{-1}, (d) 82.3 ms/25 m s^{-1}, (e) 102.9 ms/20 m s^{-1}.

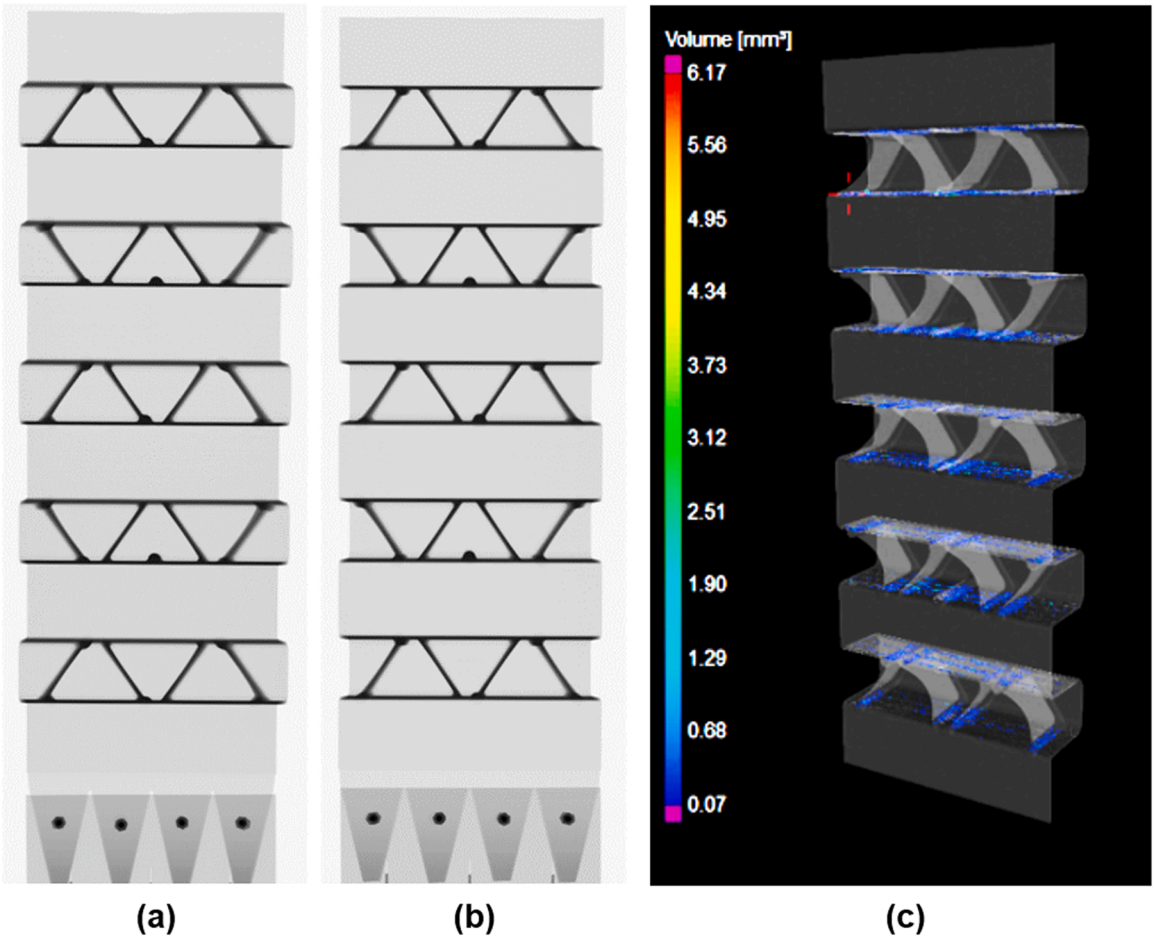

Fig. 6. (a, b) The Macro-CT micrographs showing that no large (> 0.1 mm) porosities or large inoculations, (c) 3D X-ray tomography of the castings at the die and melt temperature of 150 °C and 720 °C under the cavity fill time of 51.4 ms/in-gate velocity of 40 m s^{-1} (Scanning parameters: scanning speed (distance between two slices) 0.2 mm, resolution (pixel size) 0.4 mm.).

Severe casting defects including cracks and misruns occurred at melt temperatures lower than 720 °C and die temperatures lower than 100 °C. Fig. 7 shows the incomplete castings obtained at the melt temperature of 700 °C, with the die temperature of 200 °C and varied cavity fill time of 68.6, 51.4, 41.1 ms (in-gate velocities of 30, 40 and 50 m s^{-1}). The defects including cold shut and large porosities were readily observed even at a higher die temperature. This was due to the quick decrease of melt fluidity in contact with the low die and/or melt temperature. Also, the defects including cold shut and severe flowing marks exhibited when the in-gate velocity was lower than 30 m s^{-1}(cavity fill time larger than 68.8 ms). Moreover, the thin-wall die cavity was not able to be fulfilled at lower in-gate velocities as the melt front was freezed very quick in the narrow channels. Therefore, increasing the melt temperature and die temperature and the in-gate velocity are essential to improve the flow length in the die cavity and minimizing the casting defects. These are aligned with simulation results.

A higher die or melt temperature is beneficial for fluidity and castability which guarantee the casting integrity. However, the die soldering could readily occur at the cross-section between the flat plate and the deep rib with 90 degree turning angle when the melt temperature was increased in this specific casting. Fig. 8 shows the defects in the incomplete castings obtained at the melt temperature of 740 °C at varied die temperatures and in-gate velocities. Even at the low die temperature (100 °C), the surface flaws were often observed at both in-gate velocities of 30 and 40 m s^{-1} (cavity fill time of 68.6 and 51.4 ms). When the die temperature was increased to 150 °C, relatively large cracks, even fractures, were displayed in several locations of castings, which were not accepted for manufacturing. With the in-gate velocity of 50 m s^{-1} (cavity fill time of 41.1 ms), it was seen that the biscuit and the piston were frequently stuck together. Thus, the melt temperature should be maintained at 720 °C to achieve the fulfilment of castings without any soldering issue.

Moreover, as shown in Fig. 9a, the minor soldering issue also occurred at the first cross-section area with 90 degrees turning angle when increasing the in-gate velocity from 50 m s^{-1} to 55 m s^{-1} even at lower melt and die temperatures. Furthermore, the die soldering shown in Fig. 9b&c started to occur especially on the ribs area throughout the whole casting when increasing the die temperature from 200 °C to 220 °C at a higher in-gate velocity of 50 m s^{-1}. As a result, a successful casting could only be obtained for the die temperatures not exceeding 200 °C. Based on whole experimental results, it can be concluded that the success of casting without large viable macroscale defects can only be achieved on the castings at the melt temperature of 720 °C, die temperature of 100 °C, 150 °C and 200 °C, and in-gate velocity of 30, 40, 50 m s^{-1}. In other words, the geometry of casting is viably sound under certain casting conditions.

3.4. Microstructural characterisation

Fig. 10 presents the optical micrographs showing the size and morphology of the primary α-Al phase and micro pores in the microstructure of six casting plates extracted from the same casting part obtained at the melt temperature of 720 °C, die temperature of 200 °C, and cavity fill time of 41.1 ms (in-gate velocity of 50 m s^{-1}). Fig. 10a to f are corresponding to the microstructures of plate 1 to plate 6. Overall, all the microstructure comprised of primary α-Al phase and Al-Si eutectics with few intermetallic compounds. The primary α-Al phase exhibited two forms, i.e., coarse Al(α_1) grains nucleated in the shot sleeve with low cooling rates and the fine Al(α_2) grains formed in die cavity with high cooling rates (Zhu et al., 2021). The coarse Al(α_1) grains showed dendritic or rosette morphology, with the size being ~30–80 μm, depending on the plate positions, while the fine Al(α_2) phase displayed equiaxial grains with the size being ~5–15 μm in all the six plates. From plate 1 to plate 6, i.e. moving from the runner towards the overflow, the size and the area fraction of the coarse Al(α_1) grains became decreased, and more fine Al(α_2) grains were observed. The volume fraction was reduced from 45.15% at plate 1–8.14% at plate 6. This also confirmed that the flow speed of coarse primary Al(α_1) grains at a relatively low speed during filling the die cavity in thin and narrow channels. More importantly, this is different to the simulation results, which showed higher temperature and more liquid fraction in the areas being closer to the runner (Fig. 4). Moreover, the results revealed that the flow further away from the runner was dominated by the solidification of melt in the die cavity, thus the increased melt temperature with less coarse Al(α_1) grains is beneficial for the improvement of castability.

Porosities were the constitutional features that could be normally observed in the HPDC process due to the air entrapment in the filling process and the shrinkage during solidification (Li et al., 2015). It was seen from Fig. 10 that for the first 3 plates, no significant pores with large dimensions were present, while for the last 3 plates, several large

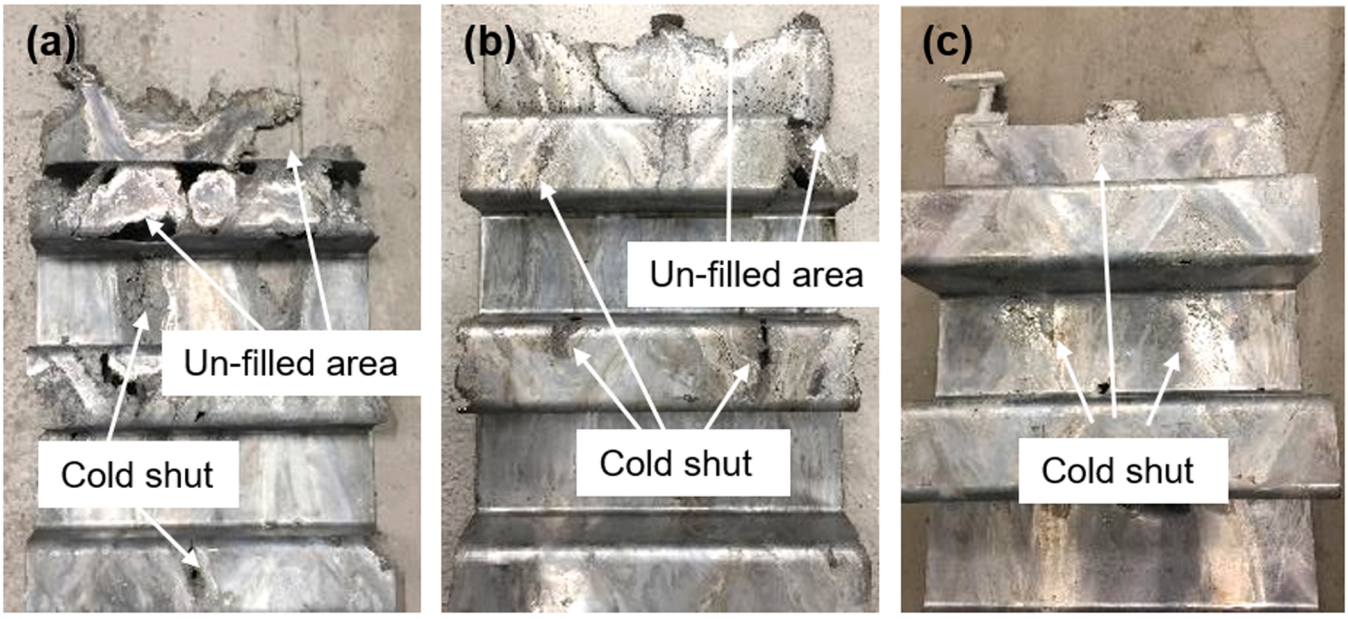

Fig. 7. The photos of incomplete castings obtained at the melt temperature of 700 °C, with the die temperature of 200 °C and the varied cavity fill time/in-gate velocities of (a) 68.6 ms/30 m s^{-1}, (b) 51.4 ms/40 m s^{-1}, and (c) 41.4 ms/50 m s^{-1}.

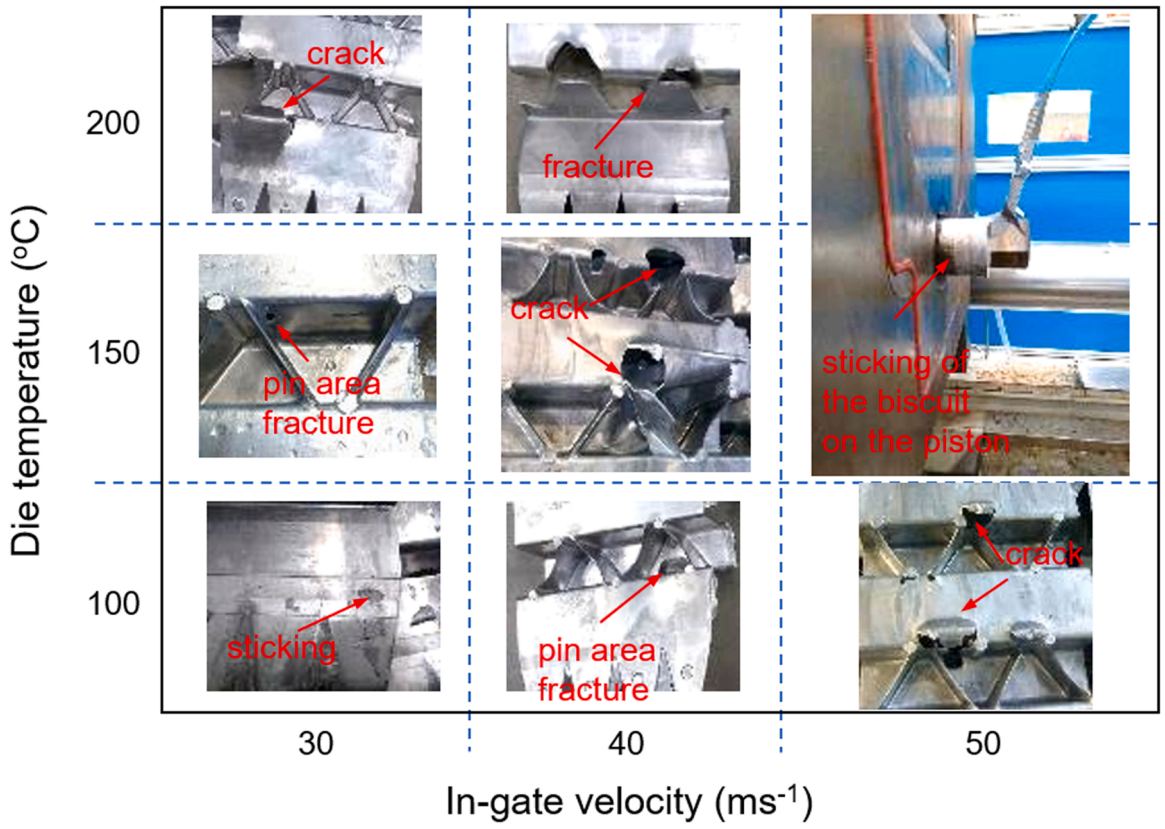

Fig. 8. The photos of incomplete castings obtained at the melt temperature of 740 °C, with varied die temperatures (100, 150 and 200 °C) and the in-gate velocities (30, 40 and 50 m s^{-1})/ cavity fill time (68.6, 51.4, 41.1 ms).

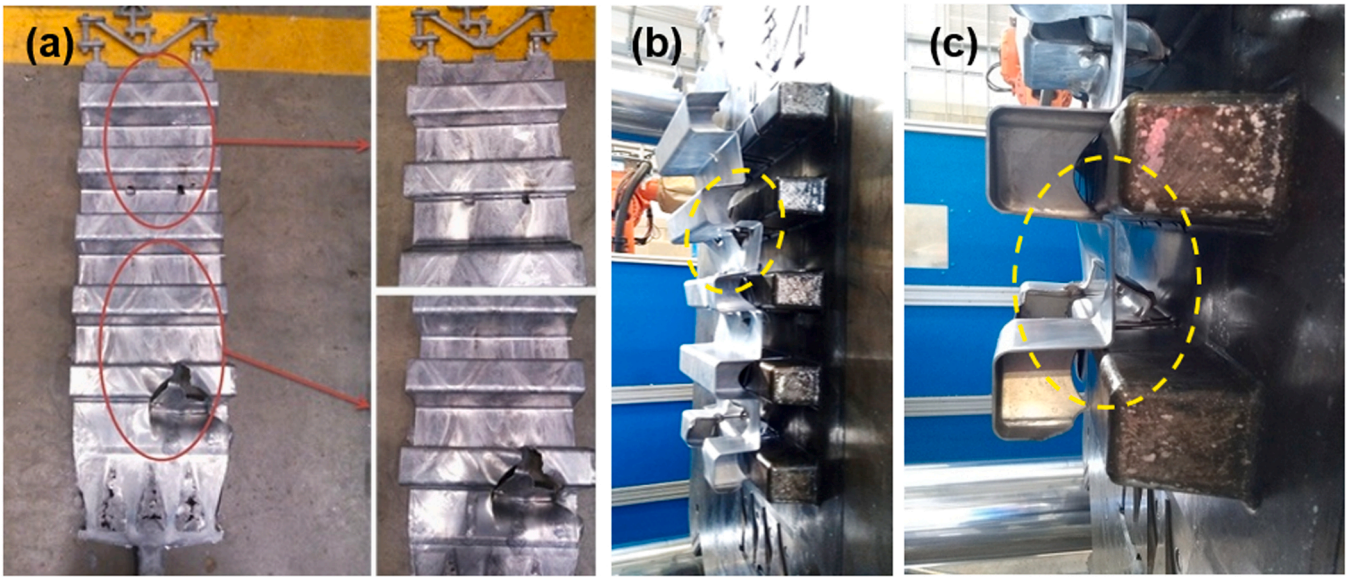

Fig. 9. The photos of the castings obtained at (a) respective melt temperature, die temperature, and the in-gate velocity of 720 °C, 100 °C, 55 m s^{-1}; and (b, c) the melt temperature, die temperature, and the in-gate velocity of 720 °C, 220 °C, 30 m s^{-1}.

pores with dimensions of ~5–10 μm were displayed, as highlighted by the dotted circles in Fig. 10d, e, &f. The increased pore size along the flow length was due to the amount of entrapped air and the cooling rate gradually increase. As a result, these large-sized pores were detrimental to the ductility of the alloy.

Fig. 11 presents the SEM micrographs showing the size and morphology of the intermetallic phases and the eutectic Si particles in the microstructure of the first plate extracted from the casting part obtained at the melt temperature of 720 °C, die temperature of 200 °C, and cavity fill time of 41.1 ms (in-gate velocity of 50 m s^{-1}). The distribution of intermetallic compounds was found relatively uniform in the microstructure as indicated by the white-contrasted particles in Fig. 11a. These intermetallic phases were identified as the coarse α-AlSiMnFe phase with the size of 10–15 μm and the fine α-AlSiMnFe phase with the

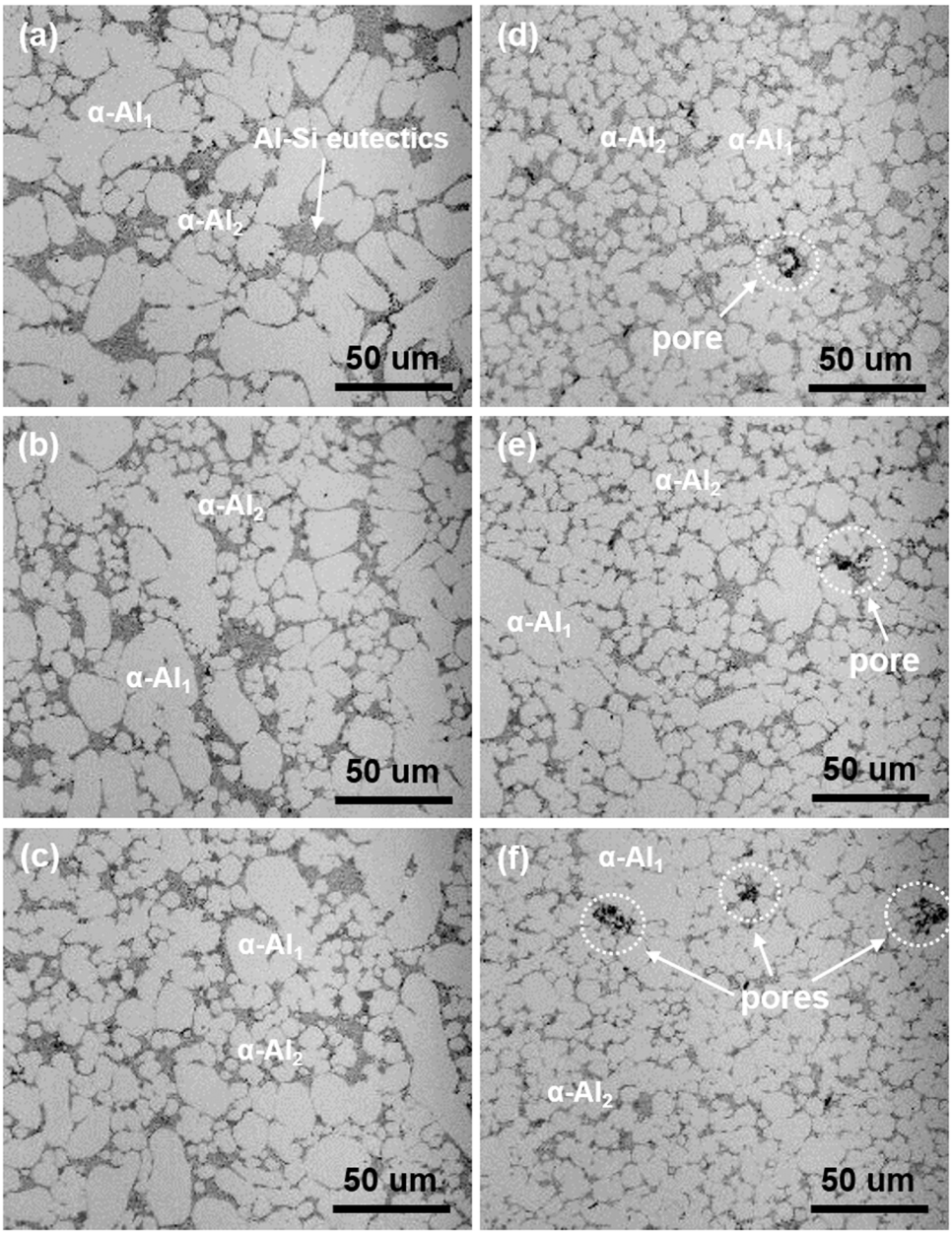

Fig. 10. Optical micrographs showing the microstructure of the 6 flat plates extracted from the casting part obtained at the process parameters: melt temperature of 720 °C, die temperature of 200 °C, and the cavity fill time of 41.1 ms (in-gate velocity of 50 m s^{-1}).

size of 0.5–2 μm. The coarse α-AlSiMnFe phase presented the blocky-shaped morphology while the fine α-AlSiMnFe phase displayed polyhedral morphology, as indicated in Fig. 11b. The coarse α-AlSiMnFe phase was formed in the shot sleeve solidification stage, usually having the coarse size and polyhedral morphology. The fine α-AlFeMnSi phase was formed in the die cavity in the pro-eutectic stage, possessing fine sizes and polyhedral or hexagonal morphology. Similar results were first reported by Ji et al. (2013) and followed by others (Zhang et al., 2019, Zhu et al., 2018) in different Al alloys. It is noted from Fig. 11b that scarce Fe elements were identified in the fine α-AlSiMn phase by the EDS (not shown here) because of the fine size of ~1 μm. This type of Mn (Fe)-bearing intermetallic phase that contained very limited Fe contents could also be formed in the pro-eutectic stage, as the majority of the Fe element was consumed at the beginning stage of solidification to form primary α-Fe. The fine α-AlSiMn showing equiaxial morphology can benefit the strength through the Orowan strengthening mechanism, especially when the particle size was less than 1 μm (Srivastava and Chaudhari, 2016). It should be noted that the needle-shaped β-Fe phase was scarcely identified in the microstructure, which was due to the sufficient Mn additions. Ji et al. (2013) have reported that an Mn/Fe ratio greater than 0.5 is preferable to favourite the transformation of Fe bearing phases from β-AlFeSi to α-AlFeMnSi, which is beneficial for the ductility of cast alloys.

3.5. Mechanical properties in as-cast castings

Fig. 12 shows the tensile properties of the plates extracted from castings obtained under different conditions. The samples were taken from the first three plates and the mean value were measured by taking the average of the first three plates of each casting in five different castings. Overall, the yield strength was in the range of 120–129 MPa and the UTS was from 243 to 260 MPa, showing a small change of ~7%. Therefore, the yield strength and UTS were not significantly dependant on the die temperatures and the in-gate velocities applied in our cases.

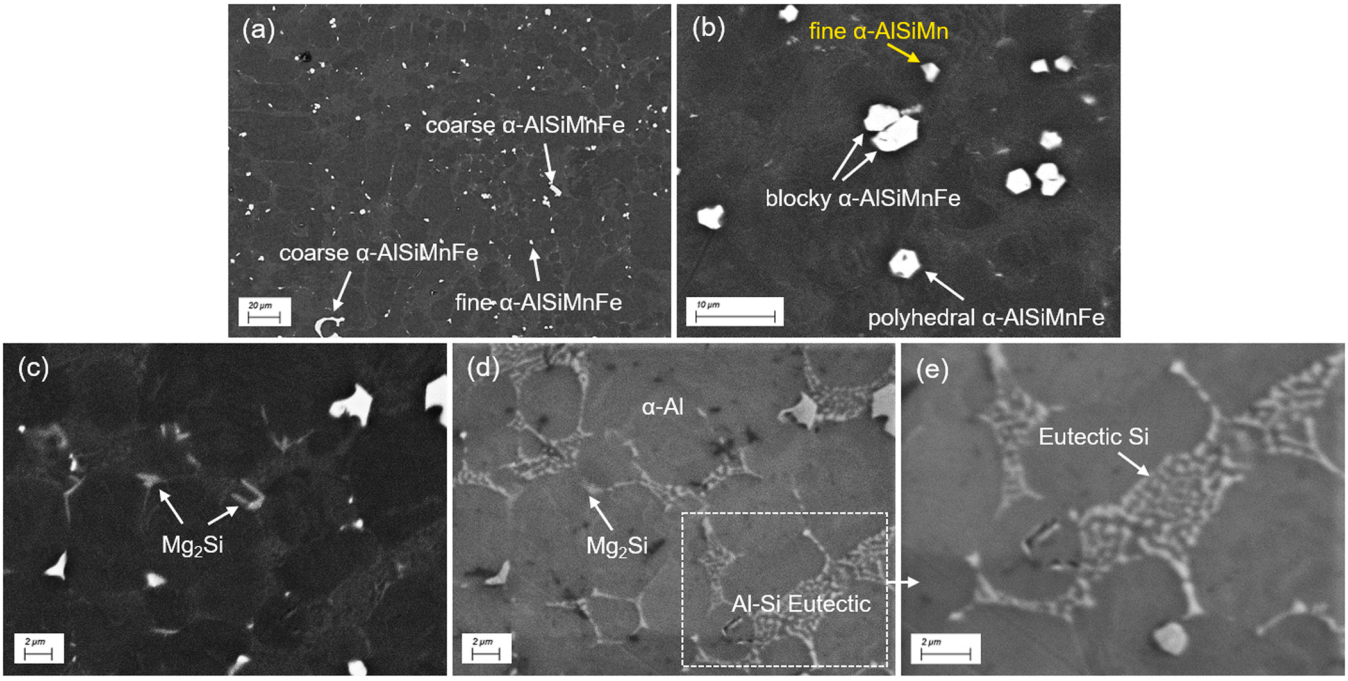

Fig. 11. SEM micrographs showing the Fe-bearing intermetallic phase, Mg_2Si intermetallic phase, and Al-Si eutectic in the microstructure of the first plates extracted from the casting part obtained at the process parameters: melt temperature of 720 °C, die temperature of 200 °C, and the cavity fill time of 41.1 ms (in-gate velocity of 50 m s^{-1}); (c) and (d) are the same area made in BSE-SEM and SE-SEM mode, respectively; (e) is extracted from the highlighted region in (d).

However, the elongation showed a great variation, being in the range of 6.7%− 12.5%, up to 87% in change.

Specifically, it is seen from Fig. 12a when the die temperature was set at 100 °C, with the in-gate velocity being 30, 40, and 50 m s^{-1} (cavity fill time of 68.6, 51.4 and 41.1 ms) the respective YS was measured to be 126.4 MPa, 126.5 MPa, and 126.7 MPa, showing nearly identical values. At the die temperature of 150 °C, the respective YS was 126.6 MPa, 124.8 MPa, and 129.7 MPa for the three in-gate velocities. When the die temperature was increased to 200 °C, the YS was measured to be 119.5 MPa, 119.4 MPa, and 128.6 MPa. In sum, the YS showed a negligible variability with the die temperature and the in-gate velocities at the constant melt temperature of 720 °C. It has been well established that for the as-cast Al alloy possessing no precipitates the YS is dominated by α-Al grain size and the secondary strengthening phase. The former strengthens the alloy by grain boundaries, allowing more boundaries in the finer grain structure to impede the dislocation movements, which is well known as the Hall-Petch mechanism by Hansen (2004) and Pereloma (2004), the latter achieves strength improvement by Orowan mechanism (Zhang and Chen, 2008), i.e. the dislocation line is looped around the hard intermetallic phase as it glides during the loading of the material, providing resistance to subsequent dislocation movement and thus increases the strength of the material. The Orowan strengthening effect increases with decreasing the size of the intermetallic phase. In the present study, the fine α-Al grains and the Mn(Fe) bearing and the eutectic Si phase are the dominant strengthening structures. The size of the α-Al and the intermetallic phase was determined by the solidification rates. When the melt temperature was fixed at 720 °C, the cooling rate of the melt was at a similar level, leading to similar sizes in α-Al grains and the intermetallic phase. In this sense, the YS values were at a similar level.

From Fig. 12b, at the die temperature of 100 °C, the UTS was 243.1, 245.0, and 249.6 MPa, seeing slight increases with the increased in-gate velocities from 30 to 50 m s^{-1}. At the die temperature of 150 °C, UTS was constantly increased from 245.0 MPa to 257.0 MPa with increasing the in-gate velocities. The same phenomenon was seen at the die temperature of 200 °C, showing the increase of the UTS from 245.7 MPa to 259.3 MPa. On the other hand, for each in-gate velocity, the UTS was slightly improved at a higher die temperature even though it was not significant. As to elongation, at the same die temperature, a higher in-gate velocity can constantly lead to a higher elongation, also when keeping the in-gate velocity as a constant, the higher die temperature caused higher elongation, as shown in Fig. 12c. The samples obtained at the die temperature of 100 °C and the cavity fill time of 68.6 ms/in-gate velocity of 30 m s^{-1} displayed the lowest elongation of 6.7%, while the sample produced at a die temperature of 200 °C and the cavity fill time of 41.1 ms/in-gate velocity of 50 m s^{-1} displayed the highest elongation of 12.5%. The variation trend for the elongation was in agreement with that for the UTS. At a higher in-gate velocity, the filling of the die cavity was improved due to a quick flow of the melt. The macro-defects such as the misruns and cold flow can be greatly relieved, thus, resulting in better elongations.

The industrial criteria of casting properties is set as yield strength > 110 MPa, UTS> 180 MPa and elongation > 10%, to achieve the optimum EFL, casting process parameters are optimised based on this standard. Fig. 13 presents the tensile properties of as-cast samples at different locations. For the first 3 plates, the mechanical properties show a good consistency or repeatability, in which the yield strength > 110 MPa, UTS> 180 MPa and elongation > 10%. For the other plates further away from the runners, the dramatic drop in the elongation and UTS occurred, although the yield strength was essentially consistent with the similar level that the first 3 plates reached. The drop of elongation was from 14.72% in plate 3–4.53% in plate 4, further to 4.98% in plate 5% and 2.77% in plate 6. A significant decrease of elongation can be attributed to the great increases in the porosity, which was confirmed in Fig. 10. The existence of large pores was prone to form stress accumulation because of the reduced loading area as weakest links, resulting in the initiation of the crack for fracture. From the results in Fig. 13, the effective flow length is limited to 525 mm, at which the yield strength is greater than 120 MPa and elongation is greater than 10%. At this point, the ratio of flow length to wall thickness is 187 for the extra-large thin-wall casting structure with the given alloy. However, if the criteria is set to be the yield strength is greater than 120 MPa and elongation is greater

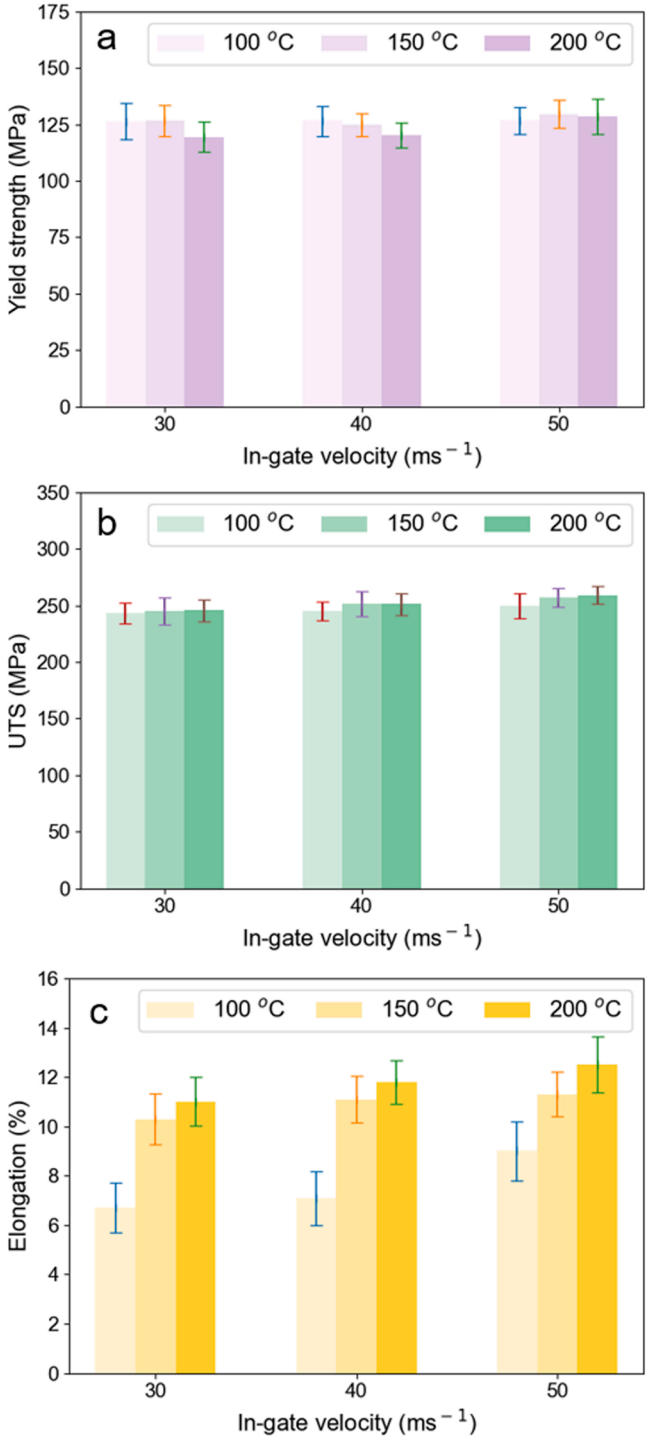

Fig. 12. The tensile properties of castings obtained at the melt temperature of 720 °C, varied die temperatures (100, 150 and 200 °C) and cavity fill time (68.6, 51.4 and 41.1 ms)/in-gate velocities (30, 40, and 50 m s^{-1}).

than 4.5%, the EFL can increase to 995 mm and the ratio of flow length to wall thickness is 355, which is increased in comparison with the previous one. The flow length is not only determined by the soundness of geometry but also determined by the criteria set for mechanical properties for extra-large thin-wall castings in high pressure die casting.

Based on the casting performance examination shown in Figs. 5–9 and properties results shown from Figs. 10 to 13, it is proposed a new concept of effective flow length (EFL) to precisely describe the castability of melt in manufacturing extra-large thin-wall castings. In

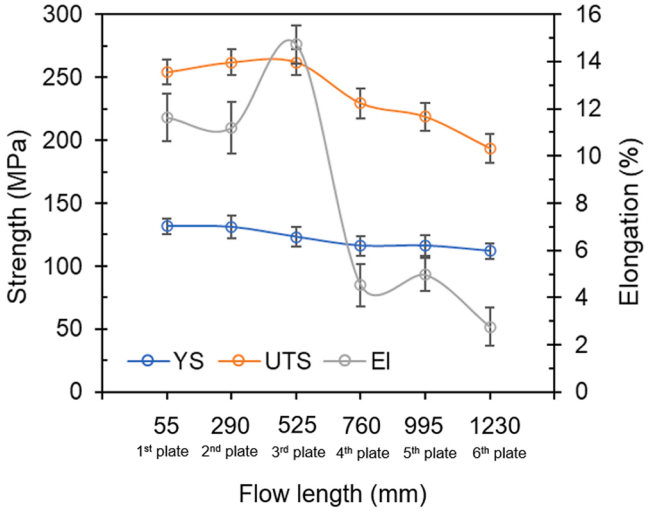

Fig. 13. The tensile results of different flow distances to the in-gate including the six plates extracted from the casting parts obtained at the melt temperature of 720 °C, die temperatures 200 °C, and cavity fill time of 41.1 ms (in-gate velocities of 50 m s^{-1}). The tensile test was conducted at room temperature.

general, castability is referred to a part design or a material property. However, it is inadequate to describe the case in high pressure die casting because (1) the significant turbulent flow causes the unstable front surface and the mechanism of blocking flow channels is no longer the same as laminal flow in conventional castings; (2) the mechanical properties in the casting is not a significant concern for high pressure die castings when the application is not under dynamic loading. However, the mechanical properties become critical with the recent development to apply high pressure die castings for the structural body. The maximum melt flow length that can achieve both acceptable casting performance microstructures and mechanical properties is defined as the EFL. In the proposed concept of EFL, both the geometrical soundness and mechanical properties in the casting body are used as the criteria of castability in high pressure die casting used for structural applications. The international, national and/or enterprise standards can be used as criteria for the requirement of mechanical properties.

4. Conclusions

The extra-large thin-wall castings with a maximum flow length of 1230 mm and a thickness of 2.8 mm were investigated by high pressure die casting in attempts to understand the effect of process parameters, including melt temperature, die temperature and shot speeds on the castability, microstructure and mechanical properties. The following conclusions can be drawn from the simulation and experimental study:

(1) The increase of melt temperature and die temperature are beneficial for the improvement in castability of making extra-large castings. The combination of the die temperature at 200 °C, the melt temperature at 720 °C and the in-gate speed at a level of 50 m s^{-1} (cavity fill time of 41.1 ms) can make sound casting to fulfil the casting geometry with a flow length of 1230 mm and a wall thickness of 2.8 mm. With the increase of melt and die temperature, defects such as die sticking are prone to form during casting. With the decrease of the melt and die temperatures, the defects such as cold shut and cold flow are likely to be formed in the castings.

(2) For the fulfilled castings, the first three plates exhibited the YS, UTS and elongation being greater than 120 MPa, 250 MPa and 10% respectively. The fourth one is 116 MPa, 230 MPa and 4.5% respectively; the fifth one is 116 MPa, 215 MPa and 5.0% respectively; and the sixth one is 110 MPa, 190 MPa and 2.5%

respectively. The heterogeneity of mechanical properties of extra-large thin-wall castings with sound geometry is the most significant concern for structural applications. This confirms that the yield strength, UTS and elongation are essentially consistent in the casting body for the flow length up to 525 mm. Beyond this length at the location further away from the gating system, the elongation is significantly decreased, although the yield strength is still not significantly changed.

(3) A new concept of effective flow length (EFL) is proposed to precisely describe the castability in high pressure die casting used for structural applications, in which both geometrical soundness and the mechanical properties in the casting body are used as the criteria of high-quality castings for structural applications. For the studied casting the EFL is approximately 525 mm when the tensile properties are set for yield strength > 120 MPa and elongation $> 10\%$, representing the ratio of flow length to the wall thickness at a level of 187. If the tensile properties are set as yield strength > 120 MPa and elongation $> 4.5\%$, the EFL can be significantly increased to 995 mm.

CRediT authorship contribution statement

Zhichao Niu: Methodology, Investigation, Validation, Formal analysis, Writing – original draft, Writing – review & editing. **Guangyu Liu:** Methodology, Formal analysis, Writing – original draft, Writing – review & editing. **Tian Li**: Methodology, Validation. **Shouxun Ji:** Funding acquisition, Conceptualization, Supervision, Writing – review & editing.

Declaration of Competing Interest

The authors declare that they have no known competing financial interests or personal relationships that could have appeared to influence the work reported in this paper.

Acknowledgement

The financial support from Innovate UK under No. 113151 is gratefully acknowledged.

References

Barkhudarov, M.R., President, V., 2009. Computer modelling simulation minimizing air entrainment in a & during slow-shot stagem Die Cast. Eng 34–37.
Cleary, P.W., Ha, J., Prakash, M., Nguyen, T., 2006. 3D SPH flow predictions and validation for high pressure die casting of automotive components. Appl. Math. Model. 30, 1406–1427.
Dong, X., Zhu, X., Ji, S., 2019. Effect of super vacuum assisted high pressure die casting on the repeatability of mechanical properties of Al-Si-Mg-Mn die-cast alloys. J. Mater. Process Technol. 266, 105–113.
Dong, X., Youssef, H., Zhang, Y., Wang, S., Ji, S., 2020. High performance Al/TiB2 composites fabricated by nanoparticle reinforcement and cutting-edge super vacuum assisted die casting process. Compos. Part B: Eng. 177, 107453.
Gunasegaram, D.R., Givord, M., O'Donnell, R.G., Finnin, B.R., 2013. Improvements engineered in UTS and elongation of aluminum alloy high pressure die castings through the alteration of runner geometry and plunger velocity. Mater. Sci. Eng. A. 559, 276–286.
Hansen, N., 2004. Hall–Petch relation and boundary strengthening. Scr. Mater. 51 (8), 801–806.
Ji, S., Watson, D., Fan, Z., White, M., 2012. Development of a super ductile diecast Al–Mg–Si alloy. Mater. Sci. Eng.: A 556, 824–833.
Ji, S., Yang, W., Gao, F., Watson, D., Fan, Z., 2013. Effect of iron on the microstructure and mechanical property of Al–Mg–Si–Mn and Al–Mg–Si diecast alloys. Mater. Sci. Eng.: A 564, 130–139.
Kong, L.X., She, F.H., Gao, W.M., Nahavandi, S., Hodgson, P.D., 2008. Integrated optimization system for high pressure die casting processes. J. Mater. Process. Technol. 201 (1–3), 629–634.
Li, X.B., Xiong, S.M., Guo, Z.P., 2015. On the porosity induced by externally solidified crystals in high-pressure die-cast of AM60B alloy and its effect on crack initiation and propagation. Mater. Sci. Eng.: A 633, 35–41.
Niu, X.P., Hua, B.H., Pinwilla, I., Li, H., 2000. Vacuum assisted high pressure die casting of aluminium alloys. J. Mater. Process. Technol. 105 (1–2), 119–127.
Rowe, J., 2012. Advanced Materials in Automotive Engineering. Woodhead Publishing Limited.
Srivastava, N., Chaudhari, G.P., 2016. Strengthening in Al alloy nano composites fabricated by ultrasound assisted solidification technique. Mater. Sci. Eng.: A 651, 241–247.
Zhang, Z., Chen, D.L., 2008. Contribution of Orowan strengthening effect in particulate-reinforced metal matrix nanocomposites. Mater. Sci. Eng.: A 483, 148–152.
Zhang, Y., Wang, S., Lordan, E., Wang, Y., Fan, Z., 2019. Improve mechanical properties of high pressure die cast Al9Si3Cu alloy via dislocation enhanced precipitation. J. Alloy. Compd. 785, 1015–1022.
Zhu, X., Dong, X., Blake, P., Ji, S., 2021. Improvement in as-cast strength of high pressure die-cast Al–Si–Cu–Mg alloys by synergistic effect of Q-Al5Cu2Mg8Si6 and θ-Al2Cu phases. Mater. Sci. Eng.: A 802, 140612.